Consistency Conditions on the Medial Axis

Anthony Pollitt¹, Peter Giblin¹, and Benjamin Kimia²

University of Liverpool, Liverpool L69 3BX, England {a.j.pollitt,pjgiblin}@liv.ac.uk
Brown University, Providence, RI, USA kimia@lems.brown.edu

Abstract. The medial axis in 3D consists of 2D sheets, meeting in 1D curves and special points. In this paper we investigate the consistency conditions which must hold on a collection of sheets meeting in curves and points in order that they could be the medial axis of a smooth surface.

1 Introduction

The Medial Axis (MA) was introduced by Blum as a representation of shape [1] in the early 1960s. Its intuitive appeal has since captured the imagination of researchers in fields where the representation of shape plays a key role, including object recognition, path planning, shape design and modelling, shape averaging, morphing shape, and meshing unorganized point samples, among many others. In many of these applications, the ability to recover the original shape from the medial axis is highly significant. In this paper we give details of constraints on the medial axis at special points, which will effect a more precise reconstruction of the original shape.

In the context of object recognition, while the early literature on the use of the medial axis is dominated by methods for computing its geometric trace, the use of a graph-based representation of the medial axis has enabled robust recognition in the face of instabilities [15,19,23]. The definition of a shape similarity metric as mediated by the skeletal graph depends in a significant way on the ability to reconstruct the shape from its medial axis [6,18]. ¹ This requires a knowledge of the constraints. Other areas where this is important include stochastic shape [13,11]; the averaging of a group of shapes, examples of which occur in medical imaging [8]; the matching of regions using 'deformable shape loci' model [16]; and industrial design [3]. Also, the field of ergonomics uses average human form measurements to optimize the interaction of people with products. The reconstruction of shape from the medial axis is also critical in robotics, where the medial axis of the free space is used for path planning [9,10].

In 2D, the medial axis of a generic planar shape consists of smooth branches with endpoints, the branches meeting in threes at points variously known as

¹ in particular in using the shock graph [18] where the graph-based geometric trace is augmented with a qualitative motion of flow; the dynamically defined shock graph is more consistent with perceptual categories of shape [20].

T. Pajdla and J. Matas (Eds.): ECCV 2004, LNCS 3022, pp. 530-541, 2004.

[©] Springer-Verlag Berlin Heidelberg 2004

Y-junctions, triple intersections or A_1^3 points; see for example [7]. Each point of the medial axis is the centre of a 'maximal' circle which is tangent to the shape boundary in at least two points, or, for endpoints of the medial axis, is tangent to the shape boundary at an extremum of curvature. Conversely, given a smooth branch γ and a 'radius' function r we can reconstruct, at any rate locally, the two corresponding parts γ^+ and γ^- of the outer boundary as an envelope of circles, centred on the smooth branch and of radius r. (See for example [6].)

However, given a connected set of smooth branches with ends and Y-junctions it is far from clear that this can be the medial axis of a shape with a smooth boundary. Even considering the local situation, it is not clear that from an arbitrary Y-junction furnished with three radius functions (agreeing at the junction point) we can expect to recover a smooth shape. In [6] it was shown that at the Y-junction there are constraints on the geometry of the three branches and on the 'dynamics', that is the derivatives of the three radius functions. One of the simplest of these constraints is

$$\frac{\kappa_1}{\sin\phi_1} + \frac{\kappa_2}{\sin\phi_2} + \frac{\kappa_3}{\sin\phi_3} = 0 \tag{1}$$

where the κ_i are the curvatures of the medial axis branches at the junction and the ϕ_i can be interpreted here as the angles between the branches (ϕ_1 is the angle between the branches with curvatures κ_2, κ_3 , etc.). (See also [5,4,21,22] for work on the relationship between the curvatures of the medial axis and the boundary.)

The constraints arise because close to a Y-junction there are two ways to use the medial axis to construct each piece of the shape boundary. Given two smooth medial axis branches γ_1, γ_2 , close to a Y-junction, and choosing orientations suitably, we reconstruct γ_1^{\pm} and γ_2^{\pm} . In this case, γ_1^{+} must agree with γ_2^{-} at the point where they meet. (See Fig. 1, left.)

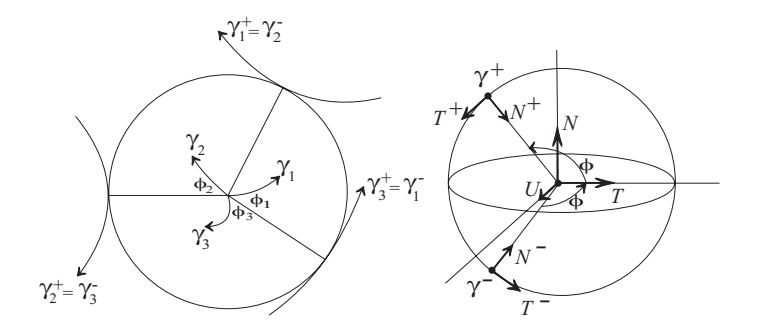


Fig. 1. Left: the A_1^3 case in 2D. Right: the 3D situation of the A_1^2 case

In this paper we take the step from 2D into 3D. The medial axis of a 3D region [2,7,12], or of the smooth surface S bounding such a region, is defined as the closure of the locus of centres of spheres tangent to S in at least two places,

only maximal spheres being considered, that is spheres whose radius equals the shortest distance from the centre to S. Using the standard notation of Fig. 2, the medial axis in 3D has sheets of A_1^2 points (ordinary tangency at two points and the centres of the spheres are maximal); curves of A_1^3 points (triple tangency) and A_3 points (edge of the medial axis where spheres have contact along a ridge); and these curves end in A_1^4 points (quadruple tangency) and A_1A_3 (or fin) points.

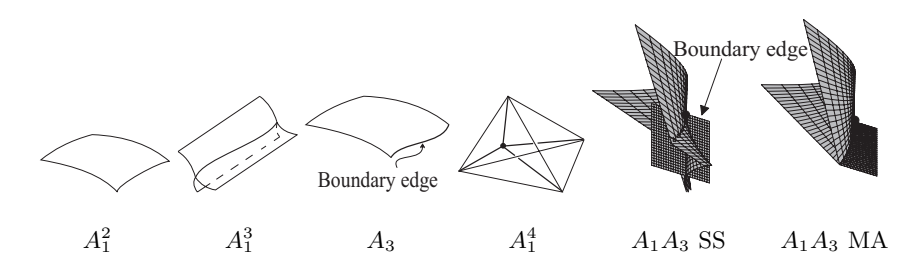


Fig. 2. The local forms of the 3D medial axis in the generic case. Thus A_1^2 is a smooth sheet, A_1^3 is a Y-junction curve, A_3 is a boundary edge of a smooth sheet, A_1^4 is a point where four A_1^3 curves lying on six sheets meet. Finally the ' A_1A_3 SS' figure shows the 'symmetry set', consisting of a swallowtail surface and a smooth sheet with boundary; this is truncated as shown in the A_1A_3 medial axis figure. The large dot marks where the boundary (A_3) edge and the Y-junction (A_1^3) curve end at the A_1A_3 point—also called a 'fin point'—itself.

This paper examines the constraints on the medial axis from a theoretical perspective; applications will follow. The results on the 3D medial axis are new; see Prop. 1, Prop. 2, (9) and Prop. 5 for the Y-junction (A_1^3) case. See Prop. 3 and (13) for A_3 , Prop. 4 for A_1^4 and Prop. 6 for A_1A_3 . See [17] for full details.

Acknowledgements. Pollitt and Giblin acknowledge the support of the British Research Council EPSRC; Giblin and Kimia acknowledge the support of NSF. The authors have also benefited greatly from conversations with Professor J. Damon.

2 The Medial Axis in Three Dimensions

We consider a smooth (A_1^2) medial axis sheet γ and its corresponding local boundary surfaces γ^+ and γ^- in 3D and quote some connected definitions and formulae from [7]. Thus spheres (radius r) centred on γ are tangent to γ^{\pm} . We have:

$$\gamma^{\pm} = \gamma - rN^{\pm} , \qquad (2)$$

where N^{\pm} is the unit normal to the boundary surface, oriented towards the centre of the bitangent sphere (i.e. tangent in at least two points). We shall assume that near a point of interest on γ the gradient of r is non-zero, and use the coordinate system given by the lines r = constant, parametrized by t, say

and referred to as 't-curves', and the gradient lines of r, parametrized by r and referred to as 'r-curves'. We can fix the (r,t) coordinate system close to $(r_0,0)$ say, by taking t to be arclength along the t-curve $r=r_0$. We denote partial derivatives by suffices.

The unit vector T is defined to be parallel to γ_r , with N a unit normal vector to the medial axis and taking $U = N \times T$ makes an orthonormal triad [T, U, N]. The velocity v is defined by:

$$\gamma_r = vT, \quad \gamma_t = wU , \qquad (3)$$

and w a function which satisfies $w(r_0,t)=1$ for all t. See Fig. 1, right. The convention of taking the boundary point γ^+ to be on the '+N' side of T and denoting ϕ to be the angle $(0<\phi<\pi)$ turned anticlockwise from T to $-N^+$, in the plane oriented by T,N, means that

$$N^{\pm} = -\cos\phi T \mp \sin\phi N$$
, $T^{\pm} = \mp \sin\phi T + \cos\phi N$, and $\cos\phi = -\frac{1}{v}$. (4)

Here the unit vector T^{\pm} is tangent to γ^{\pm} and parallel to $U \times N^{\pm}$. The equations (3), (4) hold for all points of γ .

The second order derivatives of γ at $\gamma(r_0, 0)$ are as follows.

$$\gamma_{rr} = aT - va^t U + v^2 \kappa^r N, \ \gamma_{rt} = a^t T + a^* U - v\tau^t N, \ \gamma_{tt} = -\frac{a^*}{v} T + \kappa^t N, \ (5)$$

where a, a^t, a^* are defined everywhere on γ respectively as v_r, v_t, w_r and κ^r , κ^t , and τ^t are respectively the *normal curvature* in the direction of the *r*-curve, the *normal curvature* in the direction of the *t*-curve, and the *geodesic torsion* in the direction of the *t*-curve.

3 The A_1^3 (Y-junction Curve) Case

We consider the case when the medial axis of the boundary surface S is locally three sheets, γ_1 , γ_2 , γ_3 , say intersecting in a space curve, the A_1^3 , or Y-junction, curve. Points of this curve are called Y-junction points and are centres of tritangent spheres, i.e. spheres tangent to the boundary in three points. The local boundary surfaces associated to γ_i are γ_i^{\pm} . There are six associated boundary surfaces and each coincides with one, and only one, of the others, so there are three distinct boundary surfaces. Let the identifications be $\gamma_i^+ = \gamma_{i+1}^-$, i.e. $\gamma_1^+ = \gamma_2^-$, $\gamma_2^+ = \gamma_3^-$, $\gamma_3^+ = \gamma_1^-$. This is analogous to the Y-junction case in 2D – see Fig. 1, left. Making such identifications has consequences for the geometry and dynamics of the medial sheets γ_1 , γ_2 , γ_3 . We obtain constraints by imposing conditions which use successively more derivatives. These constraints can be expressed in terms of two coordinate systems, which are as follows.

First Coordinate System. On each medial sheet γ_i there is a radius function r_i , which can be used to set up the 'grad (r_i) -coordinate system' as defined in Sect. 2 for a single A_1^2 sheet. Hence on γ_i we have

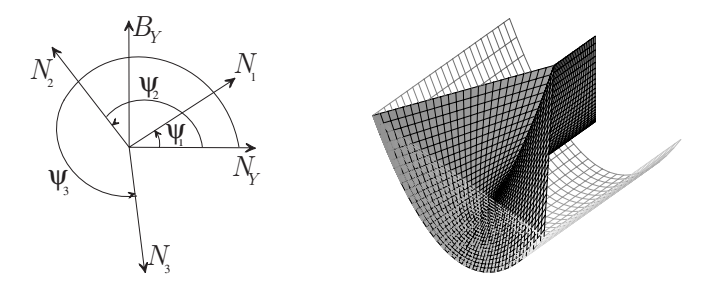


Fig. 3. Left: this is in the plane of N_Y , B_Y , respectively the principal normal and the binormal to the Y-junction curve. The unit normals N_i to the medial sheets γ_i and the angles ψ_i between N_Y and N_i are shown. Right: an example of a boundary surface consisting of a parabolic cylinder with an end and its medial axis near to a Y-junction curve. The boundary is in wireframe, the medial axis is shaded

- T_i , N_i respectively the unit tangent to the r_i -curve, unit normal to γ_i ;
- $U_i = N_i \times T_i$, the angle ϕ_i from T_i to $-N_i^+$; velocity $v_i = -1/\cos\phi_i$;
- three accelerations: a_i, a_i^t, a_i^* ;
- three 'geometries': κ_i^r , κ_i^t , τ_i^t respectively the normal curvature in the direction of the r_i -curve, and the normal curvature, geodesic torsion in the direction of the t_i -curve.

Second Coordinate System. This coordinate system is specially adapted to the Y-junction case. We set up a local Frenet frame (which will exist for generic Y-junction curves, where the curvature is non-zero) at a point $\gamma_i(r_i = r_0, t_i = 0)$ of the Y-junction curve; thus we define the following.

- T_Y , N_Y , B_Y , κ , τ are respectively the unit tangent, principal normal, binormal, curvature and torsion of the Y-junction curve;
- α_i , ψ_i are respectively the angle from T_Y to T_i , the angle from N_Y to N_i . Choose ψ_i such that $0 \le \psi_1 < \psi_2 < \psi_3 < 2\pi$ (see Fig. 3, left);
- r is the radius of the tritangent sphere centred on a Y-junction point;
- ϕ_Y is the angle between T_Y and $-N_i^{\pm}$. Choose ϕ_Y to be obtuse, corresponding to T_Y being in the direction of r increasing along the Y-junction curve;
- κ_i^W is the normal curvature of γ_i in the direction of $W_i = N_i \times T_Y$;
- ' ('prime') denotes differentiation with respect to arclength along the Y-junction curve.

The simplest constraints use the first coordinate system and are as follows (see Sect. 7 for details).

Proposition 1. At $\gamma_i(r_0,0)$ on the Y-junction curve the following holds.

$$\sum_{i=1}^{3} \left(\kappa_i^t \sin \phi_i + \frac{\kappa_i^r}{\sin \phi_i} \right) = 0 , \sum_{i=1}^{3} \left(\frac{a_i^* \kappa_i^r v_i - a_i \kappa_i^t - 2a_i^t \tau_i^t v_i}{v_i^3 \sin \phi_i} \right) = 0 .$$
 (6)

The equation on the left of (6) is a constraint only on the geometry (κ_i^r, κ_i^t) of the medial axis; it does not involve the dynamics. Compare this with the simplest constraint (1) in the 2D case.

The identifications $\gamma_i^+ = \gamma_{i+1}^-$ on the Y-junction curve and (2) mean we have $N_i^+ = N_{i+1}^-$. The normals N_i^\pm can be expressed in terms of ϕ_Y , α_i , ϕ_i and ψ_i using the second coordinate system. Then the following can be proved.

Proposition 2. At all points of the Y-junction curve, $N_i^+ = N_{i+1}^-$ for $i = 1 \dots 3$ if and only if all of the following hold.

$$\cos \phi_i = \epsilon_i \cos \phi_Y \sqrt{1 + \tan^2 \phi_Y \cos^2 \theta_i} \quad , \quad \sin \phi_i = \sin \phi_Y \sin \theta_i \quad , \tag{7}$$

$$\cos \alpha_i = \frac{\epsilon_i}{\sqrt{1 + \tan^2 \phi_Y \cos^2 \theta_i}} \qquad , \sin \alpha_i = \frac{-\tan \phi_Y |\cos \theta_i|}{\sqrt{1 + \tan^2 \phi_Y \cos^2 \theta_i}} , (8)$$

where $\theta_i = \psi_{i+2} - \psi_{i+1}$ and $\epsilon_i = \operatorname{sign}(\cos \theta_i)$.

At the second order level of derivatives we involve the geometry of the Y-junction curve to get another constraint. We can obtain expressions for κ_i^r , κ_i^t , and τ_i^t at $\gamma_i(r_0,0)$ in terms of κ , τ , κ_i^W , ψ_i' , ϕ_Y , and $\psi_{1,2,3}$. Using these expressions it can be shown that the basic constraint on the left of (6) is the same as the following.

$$\sum_{i=1}^{3} \left(\frac{\kappa_i^W \sin^2 \phi_Y - 2(\tau + \psi_i') \cos \phi_Y \sin \phi_Y \cos \theta_i + \kappa \cos^2 \phi_Y \cos \psi_i}{\sin \theta_i} \right) = 0 \quad (9)$$

For more on the Y-junction case in general, see Sect. 7. Now we consider an example of these constraints.

Example. Suppose the boundary surface to be a parabolic gutter given by $z = by^2$ and the plane x = p for b, p constants. Then a sphere whose centre lies on the A_1^3 curve has two points of contact with $z = by^2$ and one with x = p. See Fig. 3, right where b = 1, p = 0.6. The medial axis can then be calculated explicitly in terms of (x, y) for y > 0 and where (x, y, by^2) is a point on the parabolic gutter and we get

$$\gamma_1(x,y) = \left(x,0,by^2 + \frac{1}{2b}\right), \ \gamma_2(x,y) = \left(x, -y(1-2b\lambda), by^2 + \lambda\right), \ (10)$$

$$\gamma_3(x,y) = \left(x, y(1-2b\lambda), by^2 + \lambda\right), \text{ where } \lambda = \frac{p-x}{\sqrt{1+4b^2y^2}}, \tag{11}$$

$$r_1(x,y) = \frac{1}{2b}\sqrt{1+4b^2y^2}, \ r_2(x,y) = p-x, \ r_3(x,y) = p-x \ .$$
 (12)

The A_1^3 curve (which we shall call C) is given by the transversal intersection of γ_1 , γ_2 , and γ_3 . (So $1 - 2b\lambda = 0$, giving x in terms of y.)

From these parametrizations we can calculate explicitly the terms that appear in the constraints above. We can calculate formulae for ψ_i , α_i , ϕ_i , ϕ_Y in terms of y, and so we can verify (7) and (8) from Prop. 2 for this example. In a similar way we can check that (9), which is the same as the equation on the left of (6) from Prop. 1, holds in this example.

4 The A_3 Case

The A_3 case is when $\gamma^+(r_0,0) = \gamma^-(r_0,0)$ (consider Fig. 1, right – this corresponds to $\phi = 0$ or π). The corresponding points of the medial axis γ are edge points, for which the velocity v satisfies $v^2 = 1$ (see (2), (4)). We discovered the condition for the boundary surface to be smooth at an edge point $\gamma(r_0,0)$, which is as follows.

$$\frac{a}{v} - r_0 \left(\frac{aa^*}{v} + (a^t)^2 \right) \neq 0 \tag{13}$$

In the case of the medial axis γ being a general cylinder parametrized as $\gamma(u,z)=\delta(u)+z(0,0,1)=(X(u),Y(u),z)$ for δ a unit speed curve, the condition for smoothness of the boundary at a point of the z-axis where $v^2=r_u^2+r_z^2=1$ and r_0 is r at this point is

$$r_0(r_{uu}r_{zz} - r_{uz}^2) - (r_u^2r_{uu} + 2r_ur_zr_{uz} + r_z^2r_{zz}) \neq 0.$$
 (14)

Connection Between Curvatures. A parametrization of the medial axis near to an edge point can be obtained by taking the associated boundary surface S in Monge form near to an A_3 point. Let S be given by (x, y, f(x, y)) where

$$f(x,y) = \frac{1}{2}(\kappa_1 x^2 + \kappa_2 y^2) + (b_1 x^2 y + b_2 x y^2 + b_3 y^3) + (c_0 x^4 + c_1 x^3 y + \dots) + (d_0 x^5 + d_1 x^4 y + \dots) + \dots$$
(15)

(Note $b_0 = 0$ – this corresponds to A_3 along the x-direction.) Explicit calculations give the following.

Proposition 3. The limiting value (if it exists) of the Gauss curvature K (which is the product of the principal curvatures on the medial axis) as $x, y \to 0$, i.e. as we tend towards the edge point is

$$K = \frac{4(4b_2d_0 - c_1^2)\kappa_1^4}{((\kappa_1 - \kappa_2)(\kappa_1^3 - 8c_0) - 4b_1^2)^2} . \tag{16}$$

The denominator of the right hand side of (16) is only zero if $\mathbf{0}$ is an A_4 point, which we assume is not true. Equation (16) is analogous to the A_3 case in 2D (see (92) of Lemma 8 from [6].) The limiting value of K as in (16) depends on the 5-jet of the boundary in three dimensions. Equation (16) gives a criterion for K=0 on the medial axis. We can also express K in terms of derivatives of the principal curvatures κ_1 and κ_2 at (x,y)=(0,0) on the boundary (see [17]). This is also analogous to the situation in 2D.

Now consider the reconstruction of the boundary near to a ridge curve. Assume we are given the edge as a space curve, r along it, the tangent planes to γ , and the angle between the tangent to the edge and $\operatorname{grad}(r)$ at a point of the edge. Then it can be shown that we obtain the ridge curve, the tangent planes to the boundary along the ridge, the principal curvatures and principal directions of the boundary along the ridge. Compare this with (16) from Prop. 3, where very high order information about the boundary at a ridge point is required to determine second order information on the medial axis.

Local Maximum or Minimum of r **along a Ridge Curve.** It can be shown that the derivative of r with respect to arclength along the ridge is equal to zero at x = y = 0 if and only if $b_1 = 0$. Hence, using [14, pp.144], r having a local maximum or minimum on the edge is the same as κ_1 having a critical point on S.

5 The A_1^4 Case

When a sphere is tangent to the boundary surface S in four distinct points, the centre of this sphere is called an A_1^4 point. On the medial axis this corresponds to six sheets γ_i , for $i = 1 \dots 6$, intersecting in a point, which is the A_1^4 point (see Fig. 2). At this point, four Y-junction curves intersect. Each medial axis sheet contains two Y-junction curves. We can obtain constraints on the medial axis at an A_1^4 point similar to those in Sect. 3, but these are complicated and so are omitted (see [17]). Here we give a result about the reconstruction of the four boundary points.

Proposition 4 (Reconstruction at A_1^4 **Points).** At an A_1^4 point, the four contact points between the boundary surface S and a maximal sphere are determined by the directed tangents to the four Y-junction curves, pointing into the medial axis, and the radius of the sphere.

6 Radial Shape Operator

Now we shall give details of the calculations which gave the constraints of Sect. 3 and more complicated constraints which follow in the Y-junction case (Sect. 7). This section contains results connecting the geometry and dynamics of a medial axis sheet with the two corresponding boundary sheets, which are of use in Sect. 7. These results were obtained by using Damon's Radial Shape Operator S_{rad} [4] of an n-dimensional medial axis $M \subset \mathbb{R}^{n+1}$ with associated boundary B. For R a multivalued radial vector field from points of M to the corresponding points of B, with $R = rR_1$, where R_1 is a unit vector field and r is the radius function, the boundary $B = \{x + R(x) : x \in M \text{ all values of } R\}$. (In [4] U is used for our R, but for us U is already in use.) Also, in a neighbourhood of a point $x_0 \in M$ with a single smooth choice of value for R, let the radial map be given by $\psi_1(x) = x + R(x)$.

Definition 1. ([4, §1].) At a non-edge point x_0 of M with a smooth value of R, let

 $S_{\rm rad}(v) = -\operatorname{proj}_{R}\left(\frac{\partial R_{1}}{\partial v}\right)$ (17)

for $v \in T_{x_0}M$. Here proj_R denotes projection onto $T_{x_0}M$ along R. Also, $\frac{\partial R_1}{\partial v}$ is the covariant derivative of R_1 in the direction of v. The principal radial curvatures κ_{ri} are the eigenvalues of S_{rad} . The corresponding eigenvectors are the principal radial directions. Let $d\psi_t(v_i) = \frac{\partial \psi_t}{\partial v_i}$.

Now we will specialize to consider a smooth medial axis $M \subset \mathbb{R}^3$. We assume the boundary is smooth and take $-N^{\pm}$ for R_1 . We shall choose a basis \mathbf{v} for $T_{x_0}M$ and obtain the radial shape operator matrix (denoted $S_{\mathbf{v}}^{\pm}$) with respect to this basis.

Lemma 1. ([4, Theorem 3.2].) For a smooth point x_0 of M, let $x'_0 = \psi_1(x_0)$, and \mathbf{v}' be the image of \mathbf{v} for a basis $\{V_1, V_2\}$. Then there is a bijection between the principal curvatures κ_i of B at x'_0 and the principal radial curvatures κ_{ri} of M at x_0 (counted with multiplicities) given by $\kappa_i = \kappa_{ri}/(1-r\kappa_{ri})$. The principal radial directions corresponding to κ_{ri} are mapped by $d\psi_1$ to the principal directions corresponding to κ_i .

We shall choose $\{V_1, V_2\} = \{T, U\}$ to be the basis for S_{rad} of γ at $\gamma(r_0, 0)$. Then we get

$$S_{\mathbf{v}}^{\pm} = \begin{pmatrix} s_{11}^{\pm} & s_{12}^{\pm} \\ s_{21}^{\pm} & s_{22}^{\pm} \end{pmatrix} = \begin{pmatrix} -\frac{a}{v^3 \sin^2 \phi} \pm \frac{\kappa^r}{\sin \phi} \left(-\frac{a^t}{v^2} \mp \tau^t \sin \phi \right) \frac{1}{\sin^2 \phi} \\ -\frac{a^t}{v^2} \mp \tau^t \sin \phi & \frac{a^*}{v^2} \pm \kappa^t \sin \phi \end{pmatrix} . \tag{18}$$

Lemma 2. We have the following, where trace[±], det[±] respectively denote the trace, determinant of $S_{\mathbf{v}}^{\pm}$.

$$\frac{\operatorname{trace}^{+} - \operatorname{trace}^{-}}{2} = \frac{\kappa^{r}}{\sin \phi} + \kappa^{t} \sin \phi, \quad \frac{\det^{+} - \det^{-}}{2} = \frac{a^{*} \kappa^{r} v - a \kappa^{t} - 2a^{t} \tau^{t} v}{v^{3} \sin \phi} \quad (19)$$

The principal directions on γ^{\pm} can be expressed in terms of the geometry of γ by using Lemma 1.

7 The A_1^3 (Y-junction Curve) Case Continued

Now we obtain the complete set of constraints on the medial axis at a Y-junction point at the level of second order derivatives, using the results of Sect. 6. In order to equate γ_i^+ , γ_{i+1}^- up to second order derivatives we need to set $N_i^+ = N_{i+1}^-$ at Y-junction points (this gave Prop. 2) and, in addition, equate the principal curvatures and principal directions of γ_i^+ , γ_{i+1}^- at the Y-junction point $\gamma_i(r_0, 0)$.

Now we have three smooth sheets γ_i for i=1 to 3, so let $S_{\mathbf{v}_i}^{\pm}$ denote the matrix representation of the radial shape operator of γ_i corresponding to boundary γ_i^{\pm} with respect to the basis $\mathbf{v}_i = \{T_i, U_i\}$ at $\gamma_i(r_0, 0)$. Then let trace_i^{\pm} , det_i^{\pm} be the trace, determinant of $S_{\mathbf{v}_i}^{\pm}$. Hence we give each term of (19) and (18) the subscript i. We can prove the following.

Lemma 3. Equating principal curvatures on $\gamma_i^+ = \gamma_{i+1}^-$ at $(r_0, 0)$ is the same as setting trace_i⁺ = trace_{i+1}⁻ and det_i⁺ = det_{i+1}⁻.

Using Lemmas 2 and 3 we get that equating principal curvatures on $\gamma_i^+ = \gamma_{i+1}^-$ at $(r_0, 0)$ implies Prop. 1.

In order to obtain all of the information given by equating principal curvatures and principal directions, it was necessary to use the second coordinate system of Sect. 3 (involving the A_1^3 curve). This allowed us to obtain the following (full details can be found in [17]).

Proposition 5 (Constraint on Curvatures). At $\gamma_i(r_0,0)$ on the Y-junction curve the principal curvatures and principal directions of the boundaries γ_i^+ , γ_{i+1}^- for i=1, 2, 3 are equal if and only if the following holds.

$$\frac{\kappa_{i}^{W} \sin \phi_{Y}}{\sin \theta_{i}} = \frac{(\theta'_{i+1} \cos \phi_{Y} \cos 2\theta_{i+1} - \dot{\phi}_{i+1} \cos \phi_{i+1})}{\cos \theta_{i+1} \sin \theta_{i+1}} + \frac{2(\tau + \psi'_{i}) \cos \phi_{Y} \cos \theta_{i}}{\sin \theta_{i}} - \frac{(\theta'_{i+2} \cos \phi_{Y} \cos 2\theta_{i+2} - \dot{\phi}_{i+2} \cos \phi_{i+2})}{\cos \theta_{i+2} \sin \theta_{i+2}} + \frac{\kappa}{\sin \phi_{Y}} \left(\frac{\sin \psi_{i+2} \cos^{2} \phi_{i+2}}{\cos \theta_{i+2}} - \frac{\sin \psi_{i+1} \cos^{2} \phi_{i+1}}{\cos \theta_{i+1}} - \frac{\cos \psi_{i} B_{i}}{\sin \theta_{i}}\right)$$
(20)

where $B_i = \cos^2 \phi_Y + \sin^2 \phi_Y \sin^2 \theta_i$.

When the denominators of the expression above for κ_i^W are zero, we need an alternative. A point for which $\sin \theta_i = 0$ for some i is a fin (A_1A_3) point and will be covered in Sect. 8. When $\sin \phi_Y = 0$ the three points of contact on the boundary are coincident and so the sphere of contact has A_5 contact with the boundary. This case is not generic for a surface, so we ignore it. The remaining possibility is when $\cos \theta_i = 0$ for some i. See [17] for an alternative form of (20) which does not have $\cos \theta_i$ in any of the denominators involved.

Local Maximum or Minimum of r Along a Y-junction Curve. This corresponds to $\cos \phi_Y = 0$ at $\gamma_i(r_0, 0)$. Let $\cos \phi_Y = 0$ in (9) and we get

$$\sum_{i=1}^{3} \left(\frac{\kappa_i^W}{\sin \theta_i} \right) = 0 . \tag{21}$$

Compare this with (1) in two dimensions.

8 The A_1A_3 (Fin) Case

An A_1A_3 point on the medial axis is where a Y-junction curve and an A_3 curve meet and end, i.e. the A_1A_3 point is the centre of a sphere which is tangent to a surface in three places, but two of the points of contact are coincident. The medial axis near to an A_1A_3 point looks like part of a swallowtail surface with a 'fin' (another medial sheet) intersecting with the swallowtail in a curve (see Fig. 2, right). The A_1A_3 point, or fin point, is then the point where the fin meets

the other two sheets. The equation (20) holds at Y-junction points, and so it holds in the limit as two of the points coincide.

Let the coincident points of contact be γ_1^+ and γ_1^- , which means that $\sin\phi_1=0$ at the A_1A_3 point, from (2) and (4). From (7) this corresponds to $\sin\theta_1=0$, (we dismissed the possibility of $\sin\phi_Y=0$ just after Prop. 5). Therefore γ_2 and γ_3 are part of the swallowtail surface. Explicit calculations show that, as $t\to 0,\ \psi_{2,3}'\to\infty$ like 1/t and $\kappa_{2,3}^W\to\infty$ like $1/t^2$. Also $\psi_2'\sin\theta_1\to-\psi_3'\sin\theta_1$ and $\kappa_2^W\sin^2\theta_1\to-\kappa_3^W\sin^2\theta_1$, both of which are finite. The medial sheet γ_1 is smooth so κ_1^W , a_1 , a_1^t , a_1^* all remain finite as $\sin\theta_1=0$. Using these it can be shown that ϕ_Y' , $\dot{\phi}_1\sin\theta_1$, and $\psi_1'\sin\theta_1$ all remain finite as $\sin\theta_1\to0$. Then we get the limiting forms of (20) for i=1,2,3 as follows.

Proposition 6. As we tend towards a fin point along a Y-junction curve, the medial sheets must satisfy the following, where each term is finite as $\sin \theta_1 \to 0$.

$$\dot{\phi}_2 \sin^2 \theta_1 \rightarrow \dot{\phi}_3 \sin^2 \theta_1 \text{ and } (\dot{\phi}_2 - \dot{\phi}_3) \sin \theta_1 \rightarrow \text{ a finite number },$$
 (22)

$$\frac{\left(\kappa_2^W \sin^2 \theta_1\right) \sin \phi_Y}{\sin \theta_2} \to -\frac{\left(\kappa_3^W \sin^2 \theta_1\right) \sin \phi_Y}{\sin \theta_2}
\to -\frac{\dot{\phi}_2 \sin^2 \theta_1 \cos \phi_2}{\cos \theta_2 \sin \theta_2} - 2\psi_2' \sin \theta_1 \cos \phi_Y - \dot{\phi}_1 \sin \theta_1 ,$$
(23)

$$\kappa_1^W \sin \phi_Y \to \frac{\cos \phi_2}{\cos \theta_2 \sin \theta_2} \left(\dot{\phi}_3 - \dot{\phi}_2 \right) \sin \theta_1 - 2 \left(\tau + \psi_1' \right) \cos \phi_Y
+ \frac{2\psi_2' \sin \theta_1 \cos \phi_Y \cos(2\theta_2)}{\cos \theta_2 \sin \theta_2} - \frac{\kappa \cos \psi_1 \cos^2 \phi_Y}{\sin \phi_Y} .$$
(24)

See [17] for alternative forms of (23), (24) which do not have $\cos \theta_2$ in any of the denominators involved (and so are valid for $\cos \theta_i = 0$). The conclusions of Prop. 6 can be verified when the medial axis is as in the example of Sect. 3 (the fin point correponds to y = 0).

9 Summary and Conclusions

We have investigated the conditions which the geometry of the medial axis and the dynamics of the radius function must obey at singular points of the medial axis in order to obtain a consistent reconstruction of the boundary surfaces. The main case of interest is that of three sheets of the medial axis meeting in a curve (namely the locus of centres of spheres tangent to the boundary surface in three places). The constraints involve curvatures of the medial axis in two independent directions. To this extent they are reminiscent of the constraints in the 2D case which have been used in an important study of stochastic shape, among many others.

References

- 1. H.Blum, 'Biological shape and visual science', J. Theor. Biol., 38:205–287, 1973.
- 2. I.A.Bogaevsky, 'Perestroikas of shocks and singularities of minumum functions', *Physica D: Nonlinear Phenomena*, 173 (2002), 1-28.

- S.Chen & R.E.Parent, 'Shape averaging and its applications to industrial design', CGA, 9(1):47-54, 1989.
- 4. J.Damon, 'Smoothness and geometry of boundaries associated to skeletal structures II: geometry in the Blum case', to appear in *Compositio Mathematica*.
- J.Damon, 'Determining the geometry of boundaries of objects from medial data', Preprint, University of North Carolina at Chapel Hill, 2003.
- P.J.Giblin & B.B.Kimia, 'On the intrinsic reconstruction of shape from its symmetries', IEEE Transactions on Pattern Analysis and Machine Intelligence, 25 (2003), 895-911.
- P.J.Giblin and B.B.Kimia, 'A formal classification of 3D medial axis points and their local geometry', *IEEE Transactions on Pattern Analysis and Machine Intel*ligence 26 (2004), 238-251.
- 8. U.Grenander & M.Miller, 'Computational anatomy: An emerging discipline', Quarterly of Applied Mathematics, LVI(4):617–694, December 1998.
- L.Guibas, R.Holleman, & L. Kavraki, 'A probabilistic roadmap planner for flexible objects with a workspace medial axis based sampling approach', In *Proc. Intl. Conf.* Intelligent Robots and Systems, pages 254–260, Kyongju, Korea, 1999. IEEE/RSJ.
- C.Holleman & L.Kavraki, 'A framework for using the workspace medial axis in PRM planners', In *Proceedings of the International Conference on Robotics and Automation*, pages 1408–1413, San Fransisco, CA, USA, 2000.
- 11. K.Leonard, PhD. thesis, Brown University, in preparation.
- 12. F.Leymarie, '3D Shape Representation via Shock Flows', PhD. thesis, Brown University, Providence, RI, USA. See http://www.lems.brown.edu/leymarie/phd/
- 13. D.Mumford, 'The Shape of Objects in Two and Three Dimensions', Gibbs Lecture 2003, to appear in Notices of the American Mathematical Society.
- P.L.Hallinan, G.G.Gordon, A.L.Yuille, P.J.Giblin, & D.Mumford, Two- and Three-Dimensional Patterns of the Face, A K Peters, Ltd. (1999).
- 15. M.Pelillo, K.Siddiqi, & S. Zucker, 'Matching hierarchical structures using association graphs', *IEEE Trans. Pattern Analysis and Machine Intelligence*, 21(11):1105–1120, November 1999.
- 16. S.M.Pizer & C.A.Burbeck, 'Object representation by cores: Identifying and representing primitive spatial regions', *Vision Research*, 35(13):1917–1930, 1995.
- 17. A.J.Pollitt, Euclidean and Affine Symmetry Sets and Medial Axes, Ph.D. thesis, University of Liverpool. In preparation.
- T.B.Sebastian, P.N.Klein, & B.B.Kimia, 'Recognition of shapes by editing shock graphs', In *Proceedings of the Eighth International Conference on Computer Vi*sion, pages 755–762, Vancouver, Canada, July 9-12 2001. IEEE Computer Society Press.
- 19. K.Siddiqi, A.Shokoufandeh, S.Dickinson, & S.Zucker, 'Shock graphs and shape matching', *Intl. J. of Computer Vision*, 35(1):13–32, November 1999.
- K.Siddiqi, K.J.Tresness, & B.B.Kimia, 'Parts of visual form: Ecological and psychophysical aspects', *Perception*, 25:399–424, 1996.
- 21. D.Siersma, 'Properties of conflict sets in the plane', Geometry and Topology of Caustics, ed. S. Janeczko and V.M.Zakalyukin, Banach Center Publications Vol. 50, Warsaw 1999, pp. 267–276.
- 22. J.Sotomayor, D.Siersma, & R.Garcia, 'Curvatures of conflict surfaces in Euclidean 3-space', *Geometry and Topology of Caustics*, ed. S. Janeczko & V.M.Zakalyukin, Banach Center Publications Vol. 50, Warsaw 1999, pp. 277–285.
- 23. S.C.Zhu and A.L.Yuille, 'FORMS: A flexible object recognition and modeling system', *Intl. J. of Computer Vision*, 20(3):187–212, 1996.